Retrieving past geodynamic events by unlocking rock archives with μ-XRF and μ-spectroscopy

Vincent de Andrade, J. Ganne, Benoît Dubacq, C.G Ryan, F. Bourdelle, Alexis Plunder, G. Falkenberg, J. Thieme

Retrieving past geodynamic events by unlocking rock archives with µ-XRF and µ-spectroscopy

V De Andrade[1,2], J Ganne[3], B Dubacq[4,5], C G Ryan[6], F Bourdelle[7], A Plunder[4,5,8], G Falkenberg[9], J Thieme[2]

[1]Advanced Photon Source, Argonne National Laboratory, Argonne, IL 60439, USA
[2]Photon Science, Brookhaven National Laboratory, NSLS-II, Upton, NY 11793, USA
[3]IRD, UR 234, GET, Université Toulouse III, 31400 Toulouse, France
[4]UPMC Univ. Paris 06, ISTEP, UMR 7193; F-75005 Paris, France
[5]CNRS, ISTEP, UMR 7193; F-75005 Paris, France
[6]CSIRO Earth Sciences & Resource Engineering, Normanby Rd, Clayton VIC 3168, Australia
[7]GeoRessources, UMR 7359, Université de Lorraine, 54506 Vandoeuvre-lès-Nancy, France
[8]UMR CNRS 8538 Laboratoire de Géologie, ENS, 24 rue Lhomond, F-75005 Paris, France
[9]Photon Science, Deutsches Elektronen-Synchrotron DESY, Notkestr. 85, 22603 Hamburg, Germany

Email: vdeandrade@anl.gov

Abstract. Rocks are commonly polycrystalline systems presenting multi-scale chemical and structural heterogeneities inherited from crystallization processes or successive metamorphic events. This work illustrates how spatially resolved analytical techniques coupled with thermodynamic approaches allow rock compositional variations to be related to large-scale geodynamic processes. Emphasis is placed on the contribution of quantitative chemical imaging to the study of 2.2–2.0 Gy old metamorphic rocks from the West African Craton. A thorough analysis of elemental chemical maps acquired on rock thin sections enabled high pressure relic minerals to be located and re-analyzed later with precise point analyses. The pressure-temperature conditions of crystallization calculated from these analyses are typical of modern subduction zones. These results push back the onset of modern-style plate tectonics to 2.15 Gy, i.e. more than one billion years earlier than was consensually accepted. The second part of the paper describes the imaging capabilities offered by the new ultra-bright diffraction limited synchrotron sources. Experimental data acquired with the Maia detector at beamline P06 at Petra III as well as simulations of μ-XRF spectra that will be generated at the SRX beamline at NSLS-II are presented. These results demonstrate that cm^2 large chemical maps can be acquired with submicron spatial resolution and a precision suitable for thermobarometric estimates, with dwell time smaller than 1 millisecond. The last part of the paper discusses the relevance of utilizing recent X-ray fluorescence nanoprobes for diagenetic to low grade metamorphism applications.

1. Introduction

Rocks are products and witnesses of geodynamic events shaping the Earth and planetary bodies. A rock is defined by its mineralogy that is inherited from its genesis and from the successive events it encountered during its lifetime. Historically, geologists endeavor to characterize the mineralogy of rocks, from which they infer large-scale processes, for example derived from plate tectonics. With the

constant improvement of analytical tools in terms of sensitivity and spatial resolution, the apparent degree of complexity of rocks keeps increasing. The amount of information stored in rock-forming minerals is indeed extremely large, and more information about these minerals leads to a better understanding and more accurate modeling of rock-forming processes. These processes resulted in heterogeneities in the physical and chemical properties of continental crustal rocks over scales varying from the geological unit (10^2-10^3 meters) to the mineral (10^{-3}-10^{-4} meters) ; several studies within the past 10 years focused on heterogeneities occurring at the micrometer and nanometer level[1-5]. Thanks to elemental chemical imaging acquired either with electron probe micro-analyzer (EPMA), transmission electron microscope (TEM) or synchrotron X-ray fluorescence microprobe, scientists were able to characterize micrometric subdomains and the modalities of their interconnections. Combining thermodynamic models with chemical maps, it is possible to calculate the conditions of crystallization of the rock-forming minerals, which are combined to obtain high resolution pressure-temperature (P-T) paths in favorable samples[1-3, 6]. Such P-T paths are of primary importance for the understanding of geological processes. If EPMA remains one of the main analytical tool of geologists, it shows important limitations when it comes to chemical imaging, analysis of trace elements and spatial resolution below a few microns. A typical acquisition time for a single analysis of major elements is about 1 minute. Such a dwell time is incompatible with chemical imaging, where hundreds of thousands - if not millions - of analyses are required. Ultra-high brightness synchrotron X-ray fluorescence microprobes are currently the most suitable instruments to overcome the physical limitations of non-synchrotron laboratory techniques. The current light source construction projects like NSLS-II, MAX-IV or the upgrades of ESRF and APS[7] aiming for ultra-low emittance sources are about to enable very fast imaging of elements in concentration down to the sub-ppm level. The several-orders-of-magnitude gain in flux in comparison with current facilities will be also highly favorable to 3D imaging, boosting time consuming tomography techniques with a micro or nano pencil beam in combined fluorescence and diffraction mode.

The first part of this paper illustrates the contribution of micro X-ray fluorescence (μ-XRF) imaging and microspectroscopy to the study of metamorphic rocks. The second part highlights the possibilities offered by intense new generation synchrotron fluorescence microprobes like the Submicron Resolution X-ray Spectroscopy beamline[8, 9](SRX) at the National Synchrotron Light Source II (NSLS-II). Recent detector developments are also discussed. The third section focusses on the interest of zooming at the nanoscale with XRF nanoprobes while the last one concludes on radiation damage that may occur with high fluence X-ray beams.

2. Contribution of fluorescence microprobes to the study of the 2.2-2.0 Gy old West African metamorphic province

This part comments on a study[10] performed on the West African Craton (WAC). As most of the other metamorphic units in Archaean and Palaeoproterozoic cratons, WAC mainly consists of volcano-sedimentary and volcano-plutonic basins metamorphosed in greenschist facies. WAC rocks are principally composed of phyllosilicate called chlorite (chl) and phengite (phg) stable over large ranges of pressure and temperature. Previously, the lack of detailed thermodynamic data on these mineralogical phases has been a hindrance to obtaining precise and accurate P-T estimates of greenschist facies rocks. Owing to recent advances in our knowledge of the thermodynamic properties of these minerals[11-14], detailed investigations of the thermal evolution of the WAC has been possible.

Hundreds of rock thin sections were prepared from samples collected during field missions in Burkina Faso. Following visible light microscopy, tens of samples were selected to be analyzed with point EPMA analyses, while EPMA images were acquired on a few of the most promising samples. Chl and phg were preferentially analyzed. From the measured compositions, the thermodynamic multi-equilibria technique[15] can be applied. This approach checks if different mineralogical phases are in thermodynamic equilibrium and returns the P-T conditions of equilibrium, interpreted as conditions of crystallization. Below ~550ºC, it has been demonstrated that rocks do not fully re-

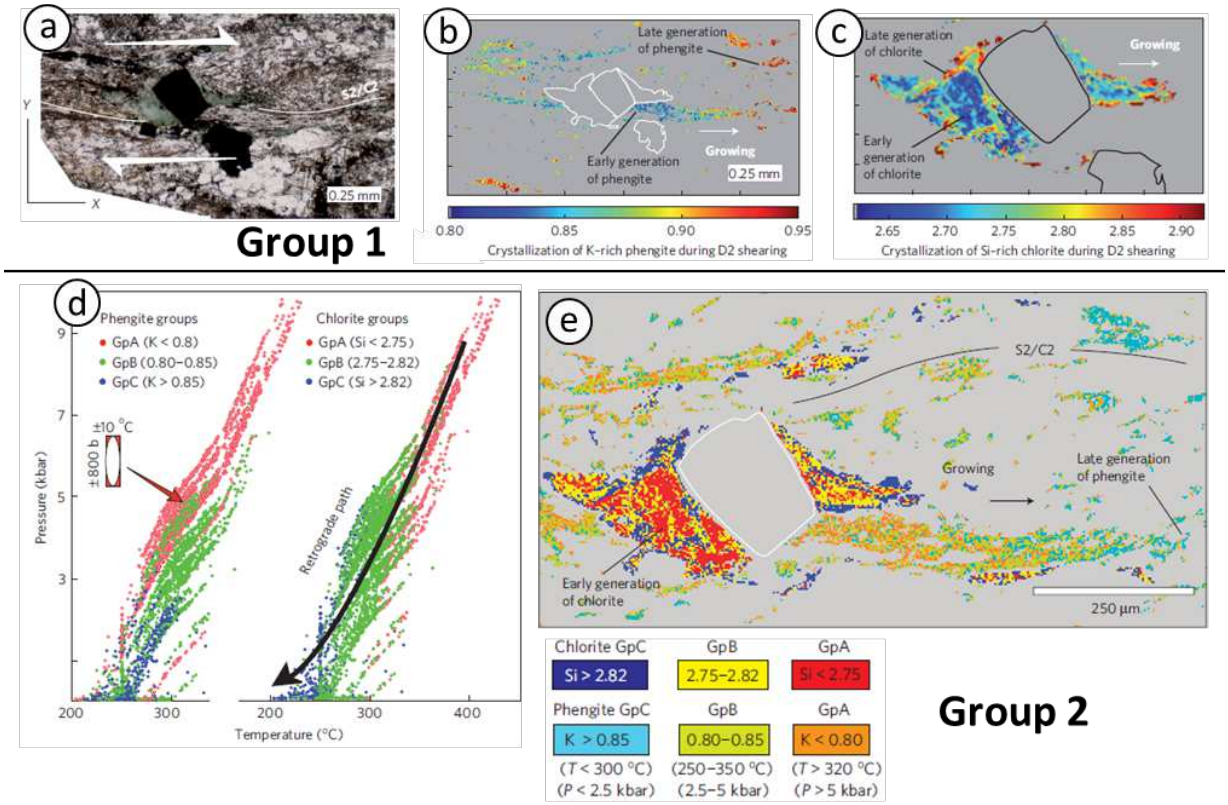

Figure 1. Group 1: Chemical evolution of chl and phg during deformation in sample Fa-33. **(a)** Photomicrograph of sample Fa-33. **(b)** Distribution of K-rich phg around a crystallization tail. **(c)** Distribution of Si-rich chl around haematite grains. Color bars correspond to the number of K & Si cations in phg **(b)** and chl (**c**). **Group 2:** P-T calculations based on chl-phg analyses. **(d)** P-T path vs K-content (left) and Si-content (right) in phg & chl. The P-T path was calculated from conventional spot analysis. **(e)** P-T maps derived from compositional images. Each chl and phg group is characterized by a specific range of composition, P & T determined in **(d)**. The Si-poor chl and K-depleted phg corresponding to the high P group A are mostly observed in the early-formed microstructures *(modified after Ganne et al., 2011)[10]*.

equilibrate. Dissolution / crystallization processes take over intra-crystalline diffusion. New crystallizations occurred locally while environmental constraints like P & T evolve. Metamorphic rocks end up as a mosaic of subdomains of different compositions whose spatial organization is a result of deformation structures, rock protolith, fluid chemistry and rock trajectory in the continental crust.

In parallel to EPMA analyses that are insensitive to the speciation of elements, μ-XANES spectra were acquired on the ID21 beamline at the ESRF to quantify the $Fe^{3+}/(Fe^{2+}+Fe^{3+})$ ratio in several chl and phg grains. The amount of Fe^{3+} incorporated in phyllosilicate varies significantly and has important consequences for the P-T calculations. A thermodynamic method allowing the inference of this ratio in chl has been proposed[2] and validated at the ESRF on the ID24 beamline, with a μ-XANES imaging approach[16]. This method has been extended here to phg and confirmed with μ-XANES spectra acquired on ID21 as control points. In some phg, the amount of Fe^{3+} is greater than 80%. Building on these new methods and considering in addition the interlayer water content in phg[11], the multi-equilibria technique was successfully applied. For most of the samples, more than a hundred P-T conditions of crystallization were returned, defining high resolution P-T paths (fig. 1d). The most remarkable results came from two samples, where the calculated pressure of crystallization reached 10-12 kb for temperatures lower than 450 ºC, and where a segment of their P-T path follows a cold thermal gradient around 10-12 ºC.km^{-1}. These conditions are typical of modern subduction zones, suggesting that modern-style plate tectonics already existed during the Palaeoproterozoic era. These

results push back the onset of modern-style plate tectonic to 2.15 Gyr, i.e. more than one billion years earlier than what was consensually accepted.

P-T path calculation of rocks from the WAC has been relatively straightforward. However, finding the relic minerals present in minute quantities and that crystallized at high P in a subduction zone has proved challenging. Amongst several hundred phg analyses, only one was in thermodynamic equilibrium with the tested chl, a result statistically not robust enough to question the date of the onset of modern-style tectonics. If the μ-XRF images obtained cover the high pressure relic minerals (fig. 1a-c), the ± 2 kb large error bars of the P-T calculations resulting from low dwell time analyses (100 ms/pixel in imaging mode) prevent drawing definitive conclusions. However, the precision of chemical maps on major elements is good enough to highlight different generations of phyllosilicates. P-T maps of crystallization have been derived from these chemical maps where the location of HP relics could be inferred out of the background noise (fig. 1e). A new set of high precision (1 minute dwell time) point analyses performed on tiny grains pre-localized on P-T maps eventually revealed the HP history of rocks.

3. Necessity for high flux fluorescence microprobes

Using modern synchrotron XRF microprobe would have been of great interest in the WAC study framework, because the high flux delivered by beamlines provides analytical precision comparable to 1 minute long point EPMA analyses, but with dwell time in the millisecond range. In the case of latest generation synchrotron sources like NSLS-II, involving state of the art fluorescence detectors, mapping of elements with sup-ppm concentrations would be feasible with millisecond dwell-time, providing that detectors are able to handle high count rates. Trace elements are of great interest in Earth Science because they provide geologists with information on large geodynamic cycles. Many trace elements also are of economic interest. Being able to map their spatial distribution in rocks will bring new light on their transport modes. The SRX beamline at NSLS-II will be equipped with two kinds of energy dispersive X-ray spectrometers (EDX). One is the Maia[17-19], a collaborative undertaking between CSIRO and Brookhaven National Laboratory. The last version of the Maia benefits from a large solid angle of 1.2 sr with 384 elements that can handle dwell time in the 10's μsecond range. With a maximum count rate of 50k counts/s/element, Maia can manage a maximum rate of 19M counts/s before saturating. The drawback of the detector is currently its average energy resolution of about 300 eV. Figures 3 and 4 show images of trace elements concentrations in a metamorphic rock containing quartz, chloritoid and garnet in addition to chl and phg[20]. Maps were acquired with the 384 version B of Maia on the P06 beamline at Petra III, with incoming beam energy set at 20.5 keV. The experimental setup uses Kirkpatrick-Baez (KB) mirrors as focusing optics with characteristics close to those of SRX (fig. 2). During the experiment, the KB focusing optics provided about 10^{12} ph/s into a 300×300 nm^2 beam spot[21]. A 4×8 mm^2 area was scanned with a 0.6 μm large beam and a 0.5 ms dwell time. The images correspond to 13332×6666 pixel^2 hyperspectral fluorescence data from which elemental composition maps were extracted using the Dynamic Analysis method[22]. The method is based on a fundamental parameters approach to μXRF quantification using the GeoPIXE software that builds a transformation matrix to project individual events into pixel concentration after following the fitting of a representative spectrum with emission lines as well as the Compton and Thomson scattering[17]. The resolution (in term of pixel number) obtained here is 43 times higher than the Blu-ray standard for instance. For such analytical conditions, detection limits are of the order of a few ppm. But it must be kept in mind that the ability to discern spatial chemical gradients also depends on relative chemical variations. The quantitative analyses forming the images of figures 3 and 4 are being studied in the framework of a large project concerning trace elements in metamorphic rocks and are not discussed here. They are exhibited here to illustrate the results scientists can expect with sub-millisecond dwell time for different trace element contents. Imaging tests were also performed on an EPMA Cameca SX100 at the ISTEP laboratory of the Paris 6 university in France.

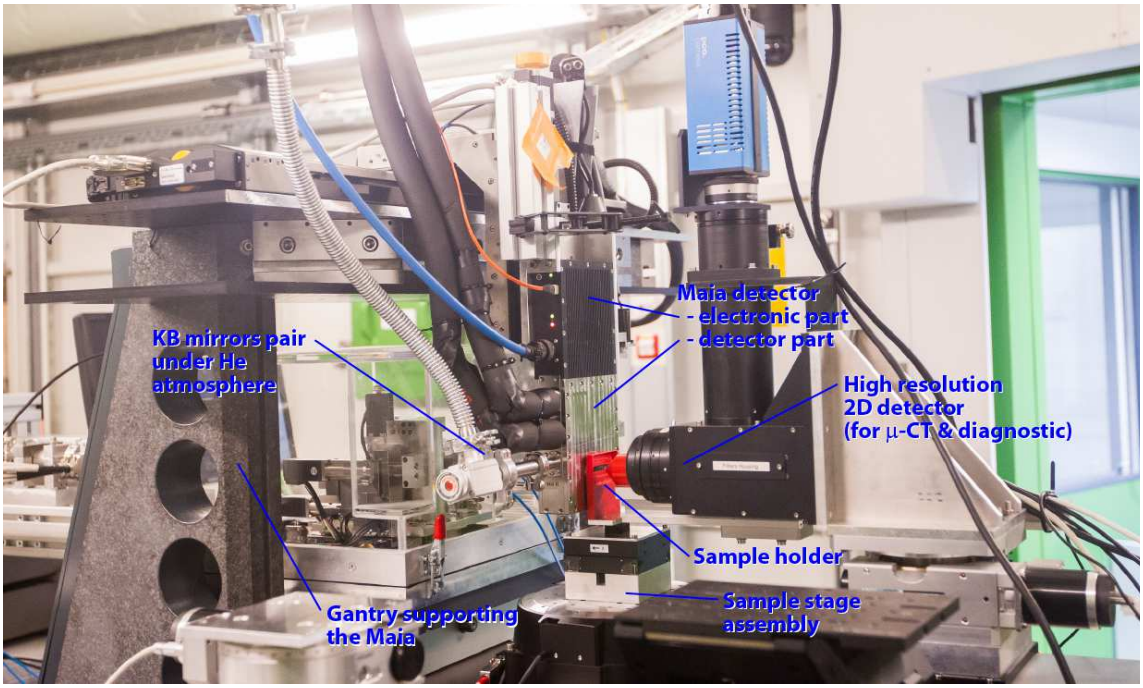

Figure 2. Experimental setup at the P06 beamline at Petra III. The Maia (384 version B) is in introduced between the KB focusing optics and the sample.

For analytical condition of 20 kV and 300 nA, a detection limit of 400-500 ppm has been reached with a dwell time of 300 ms using 4 spectrometers (~1.2 ms dwell time / spectrometer).

SRX will also operate with one ME3 and another ME4 multi-element Vortex silicon drift detector (50 mm^2 per element). Detectors will be combined with the new Quantum Xspress3 electronics, which claims a high count-rate capability providing 200, 300 and 400 eV energy resolution for photon flux of 1, 2.3 and 3 million counts per second (Mn Kα emission at ~5.9 keV). This means that the 7 elements should be able to provide 7, 16 or 21 million counts/s for energy resolution of 200, 300 or 400 eV, although a sub-ms pixel spectrum acquisition capability is yet to be demonstrated. However, the issue that remains when large elements experience high count rate is the pile-up effect for non-diluted samples like rocks. Commissioning data shows that with 3 M counts/s/element throughput on concentrated samples, background level generated with pile-up could reach about 20% of the main peaks intensity, jeopardizing trace elements detection. Z minus 1 filters have to be introduced between the sample and the detector to preferentially attenuate the most intense emission lines. For instance, a Mn foil with an absorption edge at 6.5 keV will absorb preferentially Fe K-α emission line. To summarize, Maia provides very high throughput, allowing raster scanning large areas of a square centimeter with submicron resolution and sensitivity of the order of a ppm. It can discern subtle chemico-spatial variations in a rock for a large range of elements and concentrations or locate tiny and rare particles[23] or preserved relic mineral in matrix. It also opens new paths for fluorescence μ-tomography or μ-XANES imaging spectroscopy. Megapixel hyperspectral XANES images so far only are achievable using full-field absorption imaging[24-26] can be obtained in fluorescence mode[27]. New detectors, such as the Vortex multi element arrays coupled with fast electronics also show great promise given a suitable data acquisition system.

Without considering potential radiation damages on the sample, would these detectors be able to fully sustain the outstanding flux of SRX? SRX will host in its end-station a microprobe and a nanoprobe, focusing on the sample respectively more than 10^{13} ph/s into a submicron spot and more than 10^{12} ph/s into a 50 nm spot. Both should be the most intense submicron and sub-100 nanometer

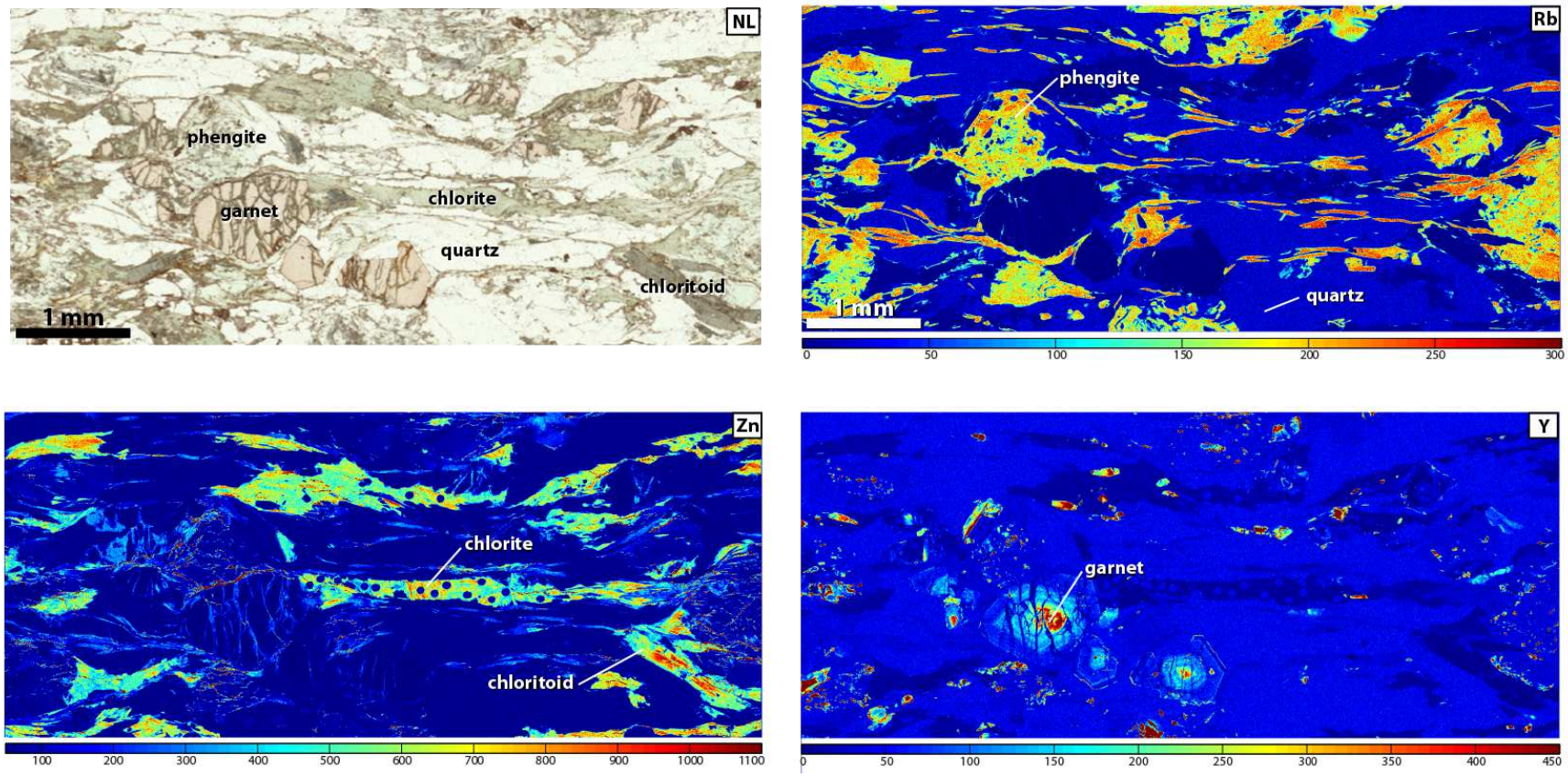

Figure 3. Quantitative images of Rb, Zn and Y concentrations acquired together with the Cr image showed in fig.4.

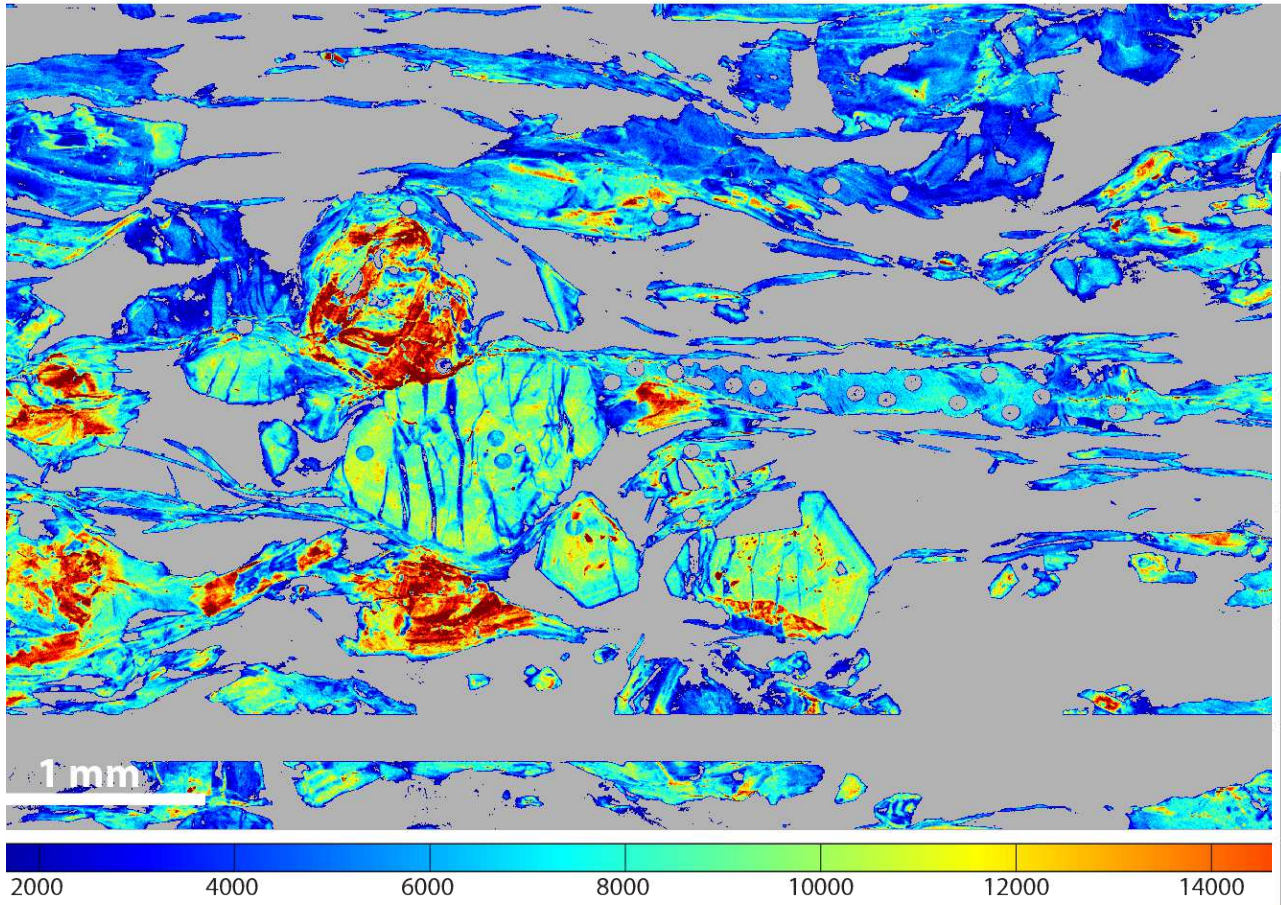

Figure 4. Quantitative image of Cr concentration (ppm) in a qtz-chl-phg-cld-gt-accessory minerals bearing metamorphic rock. This image has been

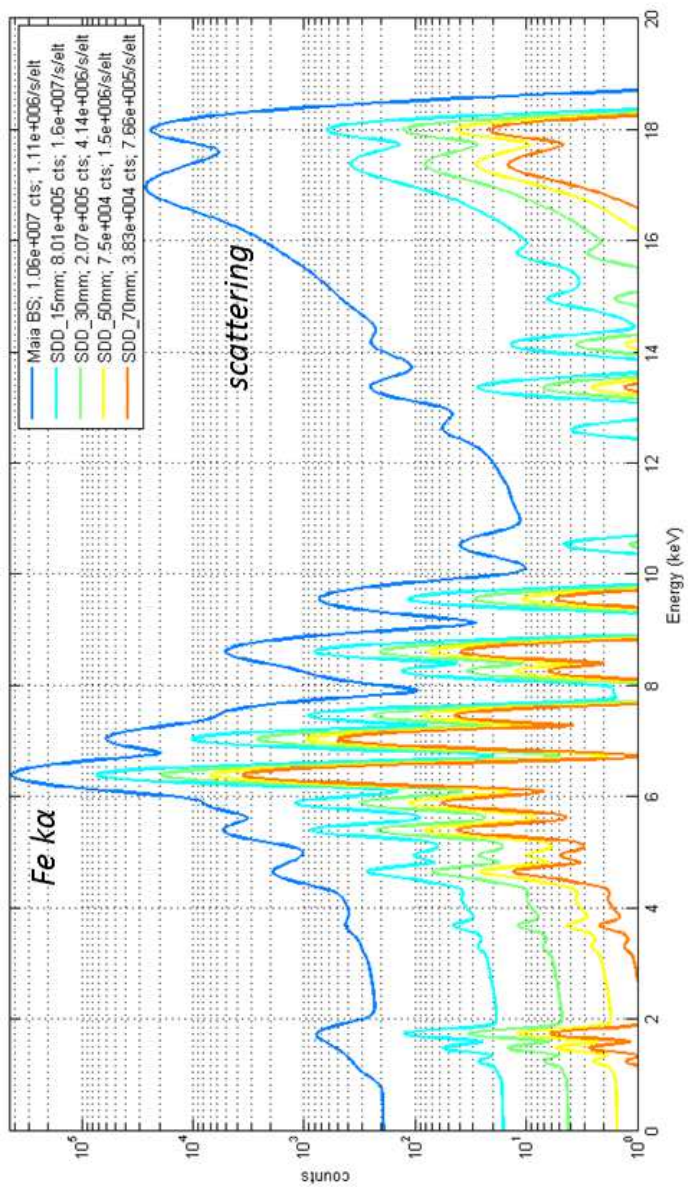

Figure 5. Fluorescence spectra simulations derived from the XMI-MSIM software[25], for a Maia

detector in backscattered geometry and a single element SDD for different working distance (15, 30, 50 and 70 mm), when operating on the SRX nanoprobe, i.e. with an incoming flux of 10^{12} ph/s. Dwell time: 50 ms. The Maia saturates at 5.10^4 ph/s, and the SDD warranty an energy resolution of 200, 300 and 400 eV for count rates of 1, 2.3 and 3M ph/s.

beams of the world. When analyzing non diluted samples, with intense major element lines, the experiment performed at Petra III on P06 beamline demonstrated that the incoming beam intensity should stay below 10^{11} ph/s to prevent detector saturation. To anticipate performances of the SRX detectors, simulations of fluorescence spectra were performed with the XMI-MSIM software[28], a Monte Carlo code dedicated to ED-XRF spectrometers including several features such as the simulation of M-lines and cascade effects. Simulations represent the Maia 384 and a single SDD element (energy resolution fixed at 200 eV) for different working distances and an incoming beam of 10^{12} ph/s as for the nanoprobe (fig. 5). The simulated sample is a 20 μm thick chl crystal. The input composition corresponds to an analyses made by laser ablation mass spectroscopy on a chl imaged in fig. 3-4. It turns out that the Maia will experience 10^6 ph/s/elt while it can only handle 5.10^4 ph/s/elt, and the SDD should move 6 cm back to operate at 1Mcts/s. Current state of the art EDX technologies are clearly a limiting factor for operating SRX at its full potential. This high flux density however offers flexibility. It allows to maintain short dwell time even for highly diluted samples, or still to work on very thin samples (<1 μm). In such cases, the amount of fluorescence emitted by thin samples drops while the spatial resolution degradation due to X-ray depth penetration is minimized.

Utilization of new wavelength dispersive spectrometers (WDS) is a credible alternative to EDX in order to benefit from the very intense beams of ultra-low emittance new synchrotron sources. With recent progresses in fabrication of polycapillary optics, compact WDS with large solid angles are now feasible and easily integrated into fluorescence microprobes[29, 30]. They provide energy resolution superior to EDX, ranging from ~5 to ~40 eV according to photon energy probed and crystal analyzers used for Bragg reflections. If these polycapillary optics based WDS designs still not sustain the comparison with recent EDX in term of efficiency, it would not saturate and not produce any pile-up with the 10^{13} ph/s flux of the SRX microprobe, and would then outclass the EDX presented earlier. However, the down side of WDS is that a full emission spectrum cannot be acquired in one shot. A continuous spectrum is obtained by rocking the analyzer and the detector. It means that one set polycapillary / analyzer / detector at fixed location in imaging mode can analyze only one element at a time.

4. Zooming from micro to nanometer scale with XRF analyses

Fluorescence nanoprobes are nowadays blooming in synchrotron facilities, especially to support research on nanomaterials, but these instruments are also relevant for metamorphic geology where tiny objects or nanoscale processes are involved. For instance, the study of small mineral inclusions, whose crystallization occurs at high P-T conditions, presents a strong interest since such objects are a window on Earth interior. Inclusions trapped in diamonds can be exhumed from locations as deep as the lower mantle[31]. Because of technical limitations, most studies have been performed so far on micro inclusions, but nanoprobes make possible to revisit samples containing nano-inclusions[32].

Nanometric spatial resolution is also particularly relevant for probing diagenetic to low grade metamorphic rocks. Indeed, mineralogical processes generally occur at the sub-micron level for relatively low temperature (T<250ºC), when slow kinetics of reactions do not permit crystallization of large grains. Phg crystallize as clay-size illite, intercalations of clays with oxides are observed in micrometric volumes. In the vein of the study described in paragraph 2, Bourdelle *et al*. interested in the compositional variations of sandstones, but using high resolution analyses acquired with transmission electron microscope (TEM) coupled with EDX[4]. As for phyllosilicate of West Africa greenstones, flakes of illite and chl contained in (low T diagenetic conditions) sandstones from the Gulf Coast in Texas exhibit compositional variations but for spatial range spanning a couple of hundreds of nanometres only. Crystals present rims around relic cores overgrowing during diagenetic

processes. From these fine scale analyses, it is then possible to apply newly developed thermobarometers involving clays[4, 11, 12] and low T chl[33, 34] to relate measured compositions to P-T conditions.

X-ray nanoprobes are still not able to compete with the sub-nanometric resolution of TEM instruments. However, obtaining reliable quantitative chemical analyses of phyllosilicate with TEM-EDX implies to reduce the power density of the beam by defocusing electrons from1 to 50 nm[4]. In this case, the expected 30 nm large X-ray beam of the SRX nanoprobe surpasses the resolution provided by TEM. More important, the acquisition time needed to get a decent signal with TEM-EDX is in the minute range. It completely annihilates imaging possibilities while on the SRX nanoprobe, dwell times can be maintained in the millisecond range to acquire high resolution large images of trace elements concentration. Also, the SRX nanoprobe will have the unique opportunity to perform XANES spectroscopy at the nanoscale with achromatic and high efficiency KB optics, offering the possibility to assess oxidation state of elements or to identify mineralogical phases with the XANES spectra "finger print" approach.

To conclude, coupling of nanoscale analyses with suitable thermobarometers offers new perspectives. In the case of metamorphic rocks, this approach reveals the end of their retrograde P-T paths (<250 ºC), i.e. the final steps of exhumation. For industrial applications, a more accurate modeling of sedimentary basins with these mineralogical tools can substantially enhance prospection efficiency of petroleum, uranium or other precious ore deposits.

5. Radiation damage considerations

Radiation damage on organic materials has been intensively studied since such compounds are easily altered by intense X-ray beams. However, effects of X-rays on hard condense matter can be observed as well, especially when submicron beams with high power density are used. Regarding SRX, the microprobe and the nanoprobe will subject samples to very high power density of about 100 and 1000 kW/mm^2 (corresponding to 1.92 mW in the nanobeam) at 12 keV. The use of such high fluence X-ray beams will necessitate extreme caution when analyzing materials to avoid any misinterpretation derived from analytical artifacts. One can cite as an example the case of S^{4+} species observed in silicate glasses. S^{4+} were first documented in natural melt inclusions in olivine of arc-related magmas[35, 36] before being identified as an instrumental artifact caused by irradiation with intense focused X-ray beams[37].

The main interaction process between X-ray beams and matter is photo-ionization yielding photoelectrons with energies lower or equal to the incident beam energy, followed by inelastic (Compton) and elastic (Rayleigh) scattering. The predominant relaxation process following the ionization is through Auger electron emission. In silicates, the travel range of electrons generated by X-ray beam below 20 keV is of the order of 1 to 2 μm. Therefore, except from a small fraction re-emitted by fluorescence or scattered, most of the absorbed energy remains in the sample[38]. Radiation damage results in oxidation state change of elements as well as mass or crystallinity loss. These effects required mechanisms for converting energy acquired by atomic electrons to kinetic energy[39]. In detail, these complex mechanisms are not always well understood and vary according to the targeted materials, the thickness of the sample, the environmental conditions, and the power density of the beam. For instance, Alkali halides are among the most radiation sensitive inorganic material whereas oxides or transition metal oxides can sustain a much higher dose before being altered by electrostatic charging[39]. In glass silicate, the use of a sub-microbeam focused with a zone plate induces photo-reduction of sulfur with the decrease S^{6+} in favor to S^{4+}. When submitted to flux two orders of magnitude higher (use of KB as focusing optics), the same sample exhibits this time photo-oxidation. Fine structure variations in a series of XANES spectra accumulated at the same sample location indicates that the S oxidation state change is coupled with reorganization of the S local structural environment[37].

Simionovici *et al.*[38] discussed radiation damage observed in silicates of the *Stardust* return samples mission. 2 μm large Mg- and Al-rich silicate grains trapped in aerogel were analyzed at the

ESRF on ID22NI with a 150 nm large pink beam with a flux of 3×10^{10} ph/s. The dose deposited with 200 ms dwell time per pixel did not damage the samples, but a comparison of subsequent XRF images of the same area acquired 8 s dwell time showed smearing of the grains along the fast scan direction and mass loss involving Mn and K. The identified damage mechanism is electrostatic charging subsequent to photoelectron and Auger electron emissions, while ionic displacement and heating processes are negligible for the analytical conditions. The power density of the SRX nanoprobe is however about 350 times higher than the one of ID22NI. It means that the dose responsible of the silicates grains radiolysis would be reached at SRX with 25 ms dwell time. In addition, to validate the assumption that heating has still negligible effects on such materials with 1 MW/mm^2, FEA are currently ongoing to establish how much the temperature would increase at the sample, either in air or in vacuum with cryogenic conditions.

After these considerations, it is clear that SRX needs a strategy to manage radiation damage even for inorganic materials. First of all, particular care must be brought to the most fragile materials, like the ones composed of alkaline elements. Hydrated materials are also very sensitive. Photoelectrons hydrolyze water making free radicals that will as a second effect produce oxidative attack. Clays and phyllosilicates comprising both alkali and water in the interlayer would be particularly subject to radiation damage. Some procedure or special sample preparation can help to circumvent this problem. For instance, in paragraph 3 is discussed the interest of working on FIB sections to minimize the spatial resolution loss due to X-ray depth penetration while decreasing the throughput on the detectors. Using sub-micron thick thin sections would also minimize the amount of absorbed Auger electrons and therefore of radiation damage. Also, when working in air, intense X-ray beams break some O_2 molecules bonds. The free O atoms recombined then with O_2 to form ozone[40]. Placing the sample in N or He atmosphere prevents the production of ozone that is a strong oxidant able to corrode sample surfaces. One general approach that SRX could adopt to deal with radiation damage could be to shorten dwell times to sub-ms levels, taking benefit of the very fast fluorescence detectors of SRX. Several frames of the same area could be acquired with 0.2 ms dwell time. This may allow enough time for charge migration and a lessening of the charge trapped gradients that drive some element loss effects (e.g. alkalis). XANES spectroscopy is a very valuable diagnostic tool for radiation damage assessment. With the help of filters, low flux XANES spectra can be measured before and after image or stationary acquisitions to track potential oxidation state (e.g. transition metal in oxides) or crystallinity changes identifiable by fine spectral modifications. In the same way, fast images with moderate flux could be performed in a first time. Comparison of peak ratio between images acquired with low and high power density would help identifying potential mass loss.

Because the degree of radiation damage experienced by materials is composition dependent, an early study of standard samples would benefit to future experiments performed at SRX. In a certain extent, those results could also be extended to Free Electron Laser instruments since interactions between hard condense matter and high fluence X-ray beam are still poorly known.

Conclusion

The use of elemental chemical imaging derived from XRF microprobes were an important milestone for the understanding of mineralogical and geodynamic processes, as is illustrated in the study of greenstones from WAC. The steady improvement of these instruments realized by the current construction or upgrade of ultra-bright diffraction limited synchrotron sources like NSLS-II opens new horizons for high speed chemical imaging of trace elements with large fields of view. Examples of acquisitions performed with the Maia 384 on a metamorphic rock underscore the achievable performances with current beamlines and EDX detectors. Simulations also show that further detector development is necessary to fully benefit from the potential of a beamline like SRX. In addition, the recent improvement in optics fabrication enables construction of efficient nanoprobes that are of interest for applications concerning low T metamorphism. However, the use of the high fluence beam of SRX necessitates strategy to control and diagnose radiation damage even on hard condense matter.

Acknowledgements
This work was financially supported by the NSLS-II project, itself funded by the US department of Energy, Office of Science and Office of Basic Energy Sciences. We are grateful to Ulrike Boesenberg and Gerd Wellenreuther from the P06 beamline team at Petra III, who helped setting up the experiment aiming to test the new Maia 384 detector. We also want to thank Robin Kirkham & Pete Siddons for their support and advices concerning the Maia. At last, thanks to Tom Schoonjans for his support in configuring the XMI-MSIM software and the SRX team endeavoring to build an outstanding instrument.

References
[1] P. Yamato, P. Agard, B. Goffé, V. De Andrade, O. Vidal, L. Jolivet, New, high-precision P-T estimates for Oman blueschists: implications for obduction, nappe stacking and exhumation processes, Journal of Metamorphic Geology, 25 (2007) 657.
[2] O. Vidal, V. De Andrade, E. Lewin, M. Muñoz, T. Parra, S. Pascarelli, P-T-deformation-Fe3+/Fe2+ mapping at the thin section scale and comparison with XANES mapping: application to a garnet-bearing metapelite from the Sambagawa metamorphic belt (Japan), Journal of Metamorphic Geology, 24 (2006) 669.
[3] V. De Andrade, O. Vidal, E. Lewin, P. O'Brien, P. Agard, Quantification of electron microprobe compositional maps of rock thin sections: an optimized method and examples, Journal of Metamorphic Geology, 24 (2006) 655.
[4] P.T. Bourdelle F., Beyssac O., Chopin C., Vidal O., Clay minerals as geo-thermometer: A comparative study based on high spatial analyses of illite and chlorite in Gulf Coast sandstones (Texas, U.S.A.), American Mineralogist, 98 (2013) 914-926.
[5] O. Vidal, T. Parra, Exhumation paths of high-pressure metapelites obtained from local equilibria for chlorite–phengite assemblages, Geological Journal, 35 (2000) 139-161.
[6] P. Lanari, O. Vidal, V. De Andrade, B. Dubacq, E. Lewin, E.G. Grosch, S. Schwartz, XMapTools: A MATLAB©-based program for electron microprobe X-ray image processing and geothermobarometry, Computers & Geosciences, (2013).
[7] E.S. Reich, Ultimate upgrade for US synchrotron, Nature, 501 (2013) 148-149.
[8] V. De Andrade, J. Thieme, P. Northrup, Y. Yao, A. Lanzirotti, P. Eng, Q. Shen, The sub-micron resolution X-ray spectroscopy beamline at NSLS-II, Nuclear Instruments and Methods in Physics Research Section A: Accelerators, Spectrometers, Detectors and Associated Equipment, 649 (2011) 46-48.
[9] V. De Andrade, J. Thieme, O. Chubar, M. Idir, Simulation and optimization of the NSLS-II SRX beamline combining ray-tracing and wavefront propagation, SPIE, In press (2011).
[10] J. Ganne, V. De Andrade, R.F. Weinberg, O. Vidal, B. Dubacq, N. Kagambega, S. Naba, L. Baratoux, M. Jessell, J. Allibon, Modern-style plate subduction preserved in the Palaeoproterozoic West African craton, Nature Geosci, 5 (2012) 60-65.
[11] B. Dubacq, O. Vidal, V. De Andrade, Dehydration of dioctahedral aluminous phyllosilicates: thermodynamic modelling and implications for thermobarometric estimates, Contributions to Mineralogy and Petrology, 159 (2010) 159-174.
[12] O. Vidal, B. Dubacq, Thermodynamic modelling of clay dehydration, stability and compositional evolution with temperature, pressure and H2O activity, Geochimica et Cosmochimica Acta, 73 (2009) 6544-6564.
[13] T. Parra, O. Vidal, P. Agard, A thermodynamic model for Fe–Mg dioctahedral K white micas using data from phase-equilibrium experiments and natural pelitic assemblages, Contrib Mineral Petrol, 143 (2002) 706-732.
[14] O. Vidal, T. Parra, F. Trotet, A Thermodynamic Model for Fe-Mg Aluminous Chlorite Using Data from Phase Equilibrium Experiments and Natural Pelitic Assemblages in the 100° to 600°c, 1 to 25 kb Range, American Journal of Science, 301 (2001) 557-592.
[15] R.G. Berman, Thermobarometry using multi-equilibrium calculations: a new technique, with petrological applications, Canadian Mineralogist, 29 (1991) 833-855.

[16] M. Muñoz, V. De Andrade, O. Vidal, E. Lewin, S. Pascarelli, J. Susini, Redox and speciation micromapping using dispersive X-ray absorption spectroscopy: Application to iron in chlorite mineral of a metamorphic rock thin section, Geochem. Geophys. Geosyst., 7 (2006) Q11020 DOI 11010.11029/12006GC001381.
[17] C.G. Ryan, D.P. Siddons, R. Kirkham, P.A. Dunn, A. Kuczewski, G. Moorhead, G. De Geronimo, D.J. Paterson, M.D. de Jonge, R.M. Hough, M.J. Lintern, D.L. Howard, P. Kappen, J. Cleverley, The New Maia Detector System: Methods For High Definition Trace Element Imaging Of Natural Material, AIP Conference Proceedings, 1221 (2010) 9-17.
[18] C.G. Ryan, D.P. Siddons, G. Moorhead, R. Kirkham, P.A. Dunn, A. Dragone, G. De Geronimo, Large detector array and real-time processing and elemental image projection of X-ray and proton microprobe fluorescence data, Nuclear Instruments and Methods in Physics Research Section B: Beam Interactions with Materials and Atoms, 260 (2007) 1-7.
[19] C. Ryan, R. Kirkham, R. Hough, G. Moorhead, D. Siddons, M. De Jonge, D. Paterson, G. De Geronimo, D. Howard, J. Cleverley, Elemental X-ray imaging using the Maia detector array: The benefits and challenges of large solid-angle, Nuclear Instruments and Methods in Physics Research Section A: Accelerators, Spectrometers, Detectors and Associated Equipment, 619 (2010) 37-43.
[20] A. Plunder, P. Agard, B. Dubacq, C. Chopin, M. Bellanger, How continuous and precise is the record of P–T paths? Insights from combined thermobarometry and thermodynamic modelling into subduction dynamics (Schistes Lustrés, W. Alps), Journal of Metamorphic Geology, 30 (2012) 323-346.
[21] C.G. Schroer, P. Boye, J.M. Feldkamp, J. Patommel, D. Samberg, A. Schropp, A. Schwab, S. Stephan, G. Falkenberg, G. Wellenreuther, Hard X-ray nanoprobe at beamline P06 at PETRA III, Nuclear Instruments and Methods in Physics Research Section A: Accelerators, Spectrometers, Detectors and Associated Equipment, 616 (2010) 93-97.
[22] C. Ryan, Quantitative trace element imaging using PIXE and the nuclear microprobe, International Journal of Imaging Systems and Technology, 11 (2000) 219-230.
[23] M. Lintern, R. Anand, C. Ryan, D. Paterson, Natural gold particles in Eucalyptus leaves and their relevance to exploration for buried gold deposits, Nat Commun, 4 (2013).
[24] B. Fayard, E. Pouyet, G. Berruyer, D. Bugnazet, C. Cornu, C. Cotte, V. De Andrade, F. Di Chiaro, O. Hignette, J. Kieffer, T. Martin, E. Papillon, M. Salomé, V.A. Sole, The new ID21 XANES full-field end-station at ESRF, Journal of Physics: Conference Series, 425 (2012) 192001.
[25] P. Beck, V. De Andrade, F.R. Orthous-Daunay, G. Veronesi, M. Cotte, E. Quirico, B. Schmitt, The redox state of iron in the matrix of CI, CM and metamorphosed CM chondrites by XANES spectroscopy, Geochimica et Cosmochimica Acta, (2012).
[26] V. De Andrade, J. Susini, M. Salomé, O. Beraldin, C. Rigault, T. Heymes, E. Lewin, O. Vidal, Submicrometer Hyperspectral X-ray Imaging of Heterogeneous Rocks and Geomaterials: Applications at the Fe K-Edge, Analytical Chemistry, 83 (2011) 4220-4227.
[27] N.J. Cook, C.L. Ciobanu, J. Brugger, B. Etschmann, D.L. Howard, M.D. de Jonge, C. Ryan, D. Paterson, Determination of the oxidation state of Cu in substituted Cu-In-Fe-bearing sphalerite via μ-XANES spectroscopy, American Mineralogist, 97 (2012) 476-479.
[28] T. Schoonjans, V.A. Solé, L. Vincze, M. Sanchez del Rio, K. Appel, C. Ferrero, A general Monte Carlo simulation of energy-dispersive X-ray fluorescence spectrometers â€" Part 6. Quantification through iterative simulations, Spectrochimica Acta Part B: Atomic Spectroscopy, 82 (2013) 36-41.
[29] M. Cotte, J. Szlachetko, S. Lahlil, M. Salome, V.A. Sole, I. Biron, J. Susini, Coupling a wavelength dispersive spectrometer with a synchrotron-based X-ray microscope: A winning combination for micro-X-ray fluorescence and micro-XANES analyses of complex artistic materials, Journal of Analytical Atomic Spectrometry, 26 1051-1059.
[30] J. Szlachetko, M. Cotte, J. Morse, M. Salome, P. Jagodzinski, J.-C. Dousse, J. Hoszowska, Y. Kayser, J. Susini, Wavelength-dispersive spectrometer for X-ray microfluorescence analysis at the X-ray microscopy beamline ID21 (ESRF), Journal of Synchrotron Radiation, 17 (2010) 400-408.

[31] M.J. Walter, S.C. Kohn, D. Araujo, G.P. Bulanova, C.B. Smith, E. Gaillou, J. Wang, A. Steele, S.B. Shirey, Deep Mantle Cycling of Oceanic Crust: Evidence from Diamonds and Their Mineral Inclusions, Science, 334 (2011) 54-57.
[32] A.M. Logvinova, R. Wirth, E.N. Fedorova, N.V. Sobolev, Nanometre-sized mineral and fluid inclusions in cloudy Siberian diamonds: new insights on diamond formation, European Journal of Mineralogy, 20 (2008) 317-331.
[33] F. Bourdelle, T. Parra, C. Chopin, O. Beyssac, A new chlorite geothermometer for diagenetic to low-grade metamorphic conditions, Contrib Mineral Petrol, 165 (2013) 723-735.
[34] A. Inoue, A. Meunier, P. Patrier-Mas, C. Rigault, D. Beaufort, P. Vieillard, Application of chemical geothermometry to low-temperature trioctahedral chlorites, Clays and Clay Minerals, 57 (2009) 371-382.
[35] N. Métrich, M. Bonnin-Mosbah, J. Susini, B. Menez, L. Galoisy, Presence of sulfite (SIV) in arc magmas: Implications for volcanic sulfur emissions, Geophysical Research Letters, 29 (2002) 33-31-33-34.
[36] M. Bonnin-Mosbah, N. Métrich, J. Susini, M. Salome, D. Massare, B. Menez, Micro X-ray absorption near edge structure at the sulfur and iron K-edges in natural silicate glasses, Spectrochimica Acta Part B: Atomic Spectroscopy, 57 (2002) 711-725.
[37] M. Wilke, P.J. Jugo, K. Klimm, J. Susini, R. Botcharnikov, S.C. Kohn, M. Janousch, The origin of S4+ detected in silicate glasses by XANES, American Mineralogist, 93 (2008) 235-240.
[38] A. Simionovici, C. Allen, S. Bajt, R. Bastien, H. Bechtel, J. Borg, F. Brenker, J. Bridges, D. Brownlee, M. Burchell, High Fluence Synchrotron Radiation Microprobe Effects on Stardust Interstellar Dust Candidates, Lunar and Planetary Institute Science Conference Abstracts, 2011, pp. 2812.
[39] R.F. Egerton, P. Li, M. Malac, Radiation damage in the TEM and SEM, Micron, 35 (2004) 399-409.
[40] C. Weilandics, N. Rohrig, N.F. Gmür, Ozone production due to synchrotron radiation, Nuclear Instruments and Methods in Physics Research Section A: Accelerators, Spectrometers, Detectors and Associated Equipment, 266 (1988) 691-698.